ISSN 1063-7761, Journal of Experimental and Theoretical Physics, 2015, Vol. 121, No. 5, pp. 828–843. © Pleiades Publishing, Inc., 2015.
Original Russian Text © A.V. Mokshin, R.M. Khusnutdinoff, A.G. Novikov, N.M. Blagoveshchenskii, A.V. Puchkov, 2015, published in Zhurnal Eksperimental'noi i Teoreticheskoi Fiziki, 2015, Vol. 148, No. 5, pp. 947–965.

SOLIDS AND LIQUIDS

Short-Range Order and Dynamics of Atoms in Liquid Gallium

A. V. Mokshin[a,b], R. M. Khusnutdinoff[a,b], A. G. Novikov[c], N. M. Blagoveshchenskii[c], and A. V. Puchkov[c]

[a] *Kazan (Volga Region) Federal University, Kazan, 420008 Russia*
[b] *Landau Institute for Theoretical Physics, Russian Academy of Sciences, Moscow, 119334 Russia*
[c] *Leypunsky Institute of Physics and Power Engineering, Obninsk, 249033 Russia*
e-mail: anatolii.mokshin@mail.ru; khrm@mail.ru

Received May 19, 2015

Abstract—The features of the microscopic structure, as well as one-particle and collective dynamics of liquid gallium in the temperature range from $T = 313$ to 1273 K, are studied on the $p = 1.0$ atm isobar. Detailed analysis of the data on diffraction of neutrons and X-rays, as well as the results of atomic dynamics simulation, lead to some conclusions about the structure. In particular, for preset conditions, gallium is in the equilibrium liquid phase showing no features of any stable local crystalline clusters. The pronounced asymmetry of the principle peak of the static structure factor and the characteristic "shoulder" in its right-hand part appearing at temperatures close to the melting point, which are clearly observed in the diffraction data, are due to the fact that the arrangement of the nearest neighbors of an arbitrary atom in the system is estimated statistically from the range of correlation length values and not by a single value as in the case of simple liquids. Compactly located dimers with a very short bond make a significant contribution to the statistics of nearest neighbors. The temperature dependence of the self-diffusion coefficient calculated from atomic dynamics simulation agrees well with the results obtained from experimental spectra of the incoherent scattering function. Interpolation of the temperature dependence of the self-diffusion coefficient on a logarithmic scale reveals two linear regions with a transition temperature of about 600 K. The spectra of the dynamic structure factor and spectral densities of the local current calculated by simulating the atomic dynamics indicate the existence of acoustic vibrations with longitudinal and transverse polarizations in liquid gallium, which is confirmed by experimental data on inelastic scattering of neutrons and X-rays. It is found that the vibrational density of states is completely reproduced by the generalized Debye model, which makes it possible to decompose the total vibrational motion into individual contributions associated with the formation of acoustic waves with longitudinal and transverse polarizations. Comparison of the heights of the low-frequency component and of the high-frequency peak in the spectral density of vibrational states also indicates a temperature of $T \approx 600$ K, at which the diffusion type of one-particle dynamics changes to the vibrational type upon a decrease in temperature. It is demonstrated that the modified Einstein–Stokes relation can be derived using the generalized Debye model.

DOI: 10.1134/S1063776115110072

1. INTRODUCTION

Gallium is a metal characterized by a specific phase diagram: in the region of the (p, T) phase diagram accessible to experimental investigations, the region of the equilibrium liquid phase is substantial [1]. For example, the melting temperature for the $p = 1.0$ atm isobar is $T_m = 302.93$ K, while the boiling point attains a value of $T_b = 2477$ K [2, 3], determining the range of the liquid phase exceeding 2000 K. Experiments on neutron [4] and X-ray [5] scattering from a gallium melt revealed a number of features indicating substantial differences between gallium and other metal systems. Namely, noticeable deviations are observed in the positions of peaks in the atomic radial distribution function $g(r)$ and in the static structure factor $S(k)$ from ideal values [6]; the asymmetry is observed in the first peak of $S(k)$, which is transformed into an "shoulder" as the temperature approaches the melting point [7]. Further, the shape of the principal peak in static structure factor $S(k)$ of liquid gallium differs from that observed for liquid alkali metals [5], for which the symmetric principal peak is successfully approximated by the Gaussian dependence [8].

An explanation of the observed peculiarities in the local structure of the gallium melt was attempted in [9]. It was proposed from an analysis of the results of atomic/molecular dynamics simulation with a pair-additive interatomic interaction potential that the asymmetry of the first peak in $S(k)$ is due to the presence of locally ordered structures (molecular clusters)

in liquid gallium. Completely different reasons that can cause the formation of the shoulder in the static structure factor for liquid gallium were given in [10], which proffered a hypothesis on the existence of covalent-type interaction apart from ion–ion interaction typical of metal melts. Nevertheless, these hypotheses have yet to be confirmed convincingly [11, 12]. In [13], it was proposed that the shoulder appears in the principal peak of $S(k)$ for a gallium melt due to so-called medium-range order, viz., structural ordering over lengths exceeding the radius of the first coordination sphere; the Friedel oscillating nature of the ion–ion interaction, which is typical of metals, can presumably facilitate this effect [14]. However, the absence of the above-mentioned singularities in the shape of $S(k)$ for other metal melts (such as Al, Pb, and Au) casts a shade of doubt on this hypothesis [15–18].

It has reliably been established that the phase diagram of gallium contains at least seven crystalline phases [19]: one thermodynamically stable phase with the orthorhombic structure, known as the Ga I or α-Ga phase, which is formed under atmospheric pressure below the melting temperature $T_m = 302.93$ K; four crystalline (β, γ, δ, and ε modifications of solid gallium), which are unstable; and two remaining crystalline structures Ga II and Ga III, which are formed only under high pressures [7].Two new crystal phases of solid gallium (*i*-Ga and κ-Ga) were detected in [20] from an analysis of experimental X-ray diffraction data. Apart from the above-mentioned polymorphism, an interesting feature of gallium as compared to other one-component systems is its ability to form the amorphous phase (glass) upon fast cooling, which is characterized by a high degree of structural disorder [21]. For example, the characteristic shoulder in the static structure factor of liquid gallium splits upon superheating. In the deep supercooling range corresponding to the amorphous phase, this shoulder is transformed into two sequential peaks [22]. It is therefore interesting to note that such a change in the shape of $S(k)$ for most one-component amorphous systems is instead associated with the second peak of the static structure factor [23–26].

Apart from the structural features of liquid gallium, considerable attention is paid to analyzing the microscopic dynamics and transport properties of this melt [27–33]. For example, the results of studying the high-frequency collective dynamics of liquid gallium at $T = 373$ K by inelastic neutron scattering were reported in [27, 34, 35]. Analysis of the shape of the spectra of dynamic structure factor $S(k, \omega)$ has made it possible to reveal two acoustic branches in the dispersion relation [28]; this was later confirmed qualitatively by experimental data on inelastic scattering of X-rays [32, 36]. The interpretation of experimental data using the "damped harmonic oscillator" model indicates that the low-frequency dispersion branch can be due to "acoustic-like" transverse oscillatory processes propagating in the melt. It should be noted that the indications of the existence of collective oscillatory processes of this type were also detected in a gallium melt at quite high pressures [33]. In spite of the vast experimental material accumulated by now, the proposed explanations of the above features of the collective and one-particle microscopic dynamics of liquid gallium (as well as other liquid metals) require additional verification using, for example, molecular dynamics calculations.

One of the goals of this study is to explain the structural features of liquid gallium manifested in the specific form of static structure factor $S(k)$, which is the quantity extracted from experimental data on elastic and inelastic scattering of neutrons and X-ray diffraction. Analysis of the experimental data on neutron scattering, calculation of the dynamic structure factor, as well as the spectral densities of the time correlation functions of longitudinal and transverse currents, which were carried via atomic dynamics simulation, revealed acoustic vibrations with longitudinal and transverse polarizations in liquid gallium. In addition, it was found that the calculated dispersion curves also agree with the experimental results on inelastic scattering of X-rays and with the results of quantum-mechanical simulation. We consider one-particle translational dynamics responsible for self-diffusion, as well as the vibrational dynamics of particles. We show that high-frequency singularities in the vibrational density of states are due to the vibrational dynamics of particles participating in the formation of acoustic-like collective excitations with longitudinal and transverse polarizations. The form of the vibrational density of states can be reproduced unambiguously using the generalized Debye model.

2. SIMULATION DETAILS

Liquid gallium was simulated by the atomic/molecular dynamics method at a temperature of $T = 313$ K ($T_m \approx 303$ K). The system consisted of $N = 13\,500$ atoms located in a cubic cell with periodic boundary conditions. The interaction between gallium atoms was based on the embedded atom method (EAM potential) [37, 38]. Apart from conventional paired interatomic interactions, multiparticle interactions are introduced in a certain way in EAM potentials [39]. For example, the potential energy for metals described by EAM potentials can be written as

$$\mathcal{U}(r) = \sum_{i<j} \varphi(r_{ij}) + \sum_i \Phi(\rho_i). \quad (1)$$

Here, $\varphi(r_{ij})$ is the pair interatomic interaction potential and $\Phi(\rho_i)$ is the "embedded" potential effectively characterizing the multiparticle interactions in terms of the electron density of the *i*th atom (i.e., ρ_i). The simulation was carried out in an isobaric–isothermal (*NpT*) ensemble. To keep the system in thermodynamic equilibrium, we used a Nosé–Hoover thermo-

stat and barostat with the interaction parameter τ = 100.00 ps [40]. The equations of motion for atoms were integrated using the velocity Verlet algorithm with a time step of $dt = 10^{-15}$ s [41]. The gallium melt samples were obtained at temperatures of T = 313, 400, 500, 600, 700, 823, 900, 1073, and 1273 K at a pressure of p = 1.0 atm. To bring the system to equilibrium, 10^6 time steps were made in each (p, T) state in the NpT ensemble and 1.2×10^6 steps in the NVT ensemble for calculating temporal and spectral characteristics.

3. EXPERIMENTAL

The experiment on neutron scattering in liquid gallium was carried out with a DIN-2PI time-of-flight spectrometer (IBR-2 reactor, Dubna) with an initial neutron energy of E_0 = 7.65 meV [34, 35, 42]. The energy resolution of the spectrometer was $\Delta E_0 \sim$ 0.5 meV for wavenumbers comparable to k = 2.5 Å^{-1}, which approximately corresponds to the principal maximum approximation in static structure factor $S(k)$. The interval of wavenumbers k was (0.3–2.7) Å^{-1}.

To analyze the experimental data, we decomposed the scattering law into partial components associated with different types of neutron scattering from liquid gallium: quasi-elastic coherent and quasi-elastic incoherent scattering, inelastic coherent and inelastic incoherent scattering, and multiple scattering. The corresponding decompositions into the components of the scattering law were performed with the relevant software [43]. The self-diffusion coefficient in the gallium melt was estimated from analysis of the quasi-elastic scattering data. The coherent quasi-elastic component was considered for the wavenumber corresponding to the position of the principal maximum $k_m \approx$ 2.5 Å^{-1} in the static structure factor $S(k)$, while the incoherent quasi-elastic component was considered for the range of wavenumbers $k <$ 1.2 Å^{-1} (i.e., small scattering angles at which the coherence effects are negligibly small). For example, the self-diffusion coefficient was calculated using the modified hard sphere model [44] employed for describing the dependence of width $\Delta\omega$ of coherent quasi-elastic peaks on wavenumber k and temperature T. In addition, the self-diffusion coefficient was determined in a different way, in which the widths of the peaks in incoherent quasi-elastic scattering were interpreted using Fick's law of diffusion. As a result, the temperature dependence of the self-diffusion coefficient was determined in the temperature interval $T \in$ [320 K; 793 K] (see Section 5).

Experimental scattering data were used to estimate the dispersion curves characterizing high-frequency collective excitations in liquid gallium. For this purpose, we analyzed the spectra of dynamic structure factor $S(k, \omega)$, which is connected with the intensity $I(k, \omega)$ of inelastic coherent neutron scattering by the relation

$$I(k,\omega) \propto \int R(k,\omega')S(k,\omega-\omega')d\omega'$$

where $R(k, \omega)$ is the experimental resolution function. From the positions of the peaks and singularities in the $S(k, \omega)$ spectra, we established the existence of two high-frequency modes and calculated the corresponding dispersion curves (see Section 6).

4. STRUCTURAL FEATURES OF GALLIUM MELT

4.1. Radial Distribution of Particles and Structure Factor

Information on the mutual arrangement of particles in the system is contained in the static structure factor

$$S(\mathbf{k}) = 1 + \rho\int \exp(-i\mathbf{k}\cdot\mathbf{r})[g(\mathbf{r})-1]d\mathbf{r}, \qquad (2)$$

which is a quantity directly measured in experiments on neutron and X-ray diffraction [45]. Here, $\rho = N/V$ is the number density, $g(\mathbf{r})$ is the radial distribution function, $\mathbf{k}$ is the wavevector, and $\mathbf{r}$ is the radius vector characterizing the mutual arrangement of particles in an arbitrary pair. In the absence of preferred directions, which is usual for disordered systems such as liquids or amorphous materials, it is possible to ignore the dependence on the direction of the probe particles (beams) relative to the sample ignored. This enables us to write expression (2) in the form

$$\begin{aligned} S(k) &= 1 + \frac{4\pi\rho}{k}\int_0^\infty r[g(r)-1]\sin(kr)dr \\ &= 1 - \frac{4\pi\rho}{k}\frac{d}{dk}\int_0^\infty [g(r)-1]\cos(kr)dr, \end{aligned} \qquad (3)$$

where $k = |\mathbf{k}|$ is the wavenumber. It can be seen from Eq. (3) that static structure factor $S(k)$ can be related to the radial distribution function $g(r)$ in terms of Fourier sine- or cosine-transform.

In a simple equilibrium liquid, $g(r)$ is a damped function oscillating at about a unit value of $g(r) = 1$. As a rule, the first three or four peaks can be distinguished visually [8]. This is manifested most clearly for liquids with high densities at temperatures close to melting point T_m. The positions of the peaks in $g(r)$ correspond to the characteristic correlation lengths of short- and medium-range order, which indicate the radii of coordination spheres (r_1 of the first, r_2 of the second, r_3 of the third, etc., spheres) in the case of crystalline systems. Remarkably, radial distribution function $g(r)$ and the static structure factor $S(k)$ corresponding to it have analogous structures: in static structure factor $S(k)$, the principal (first) peak k_m is also observed, and the oscillating tail of $S(k)$ tends to a value of $S(k) = 1$

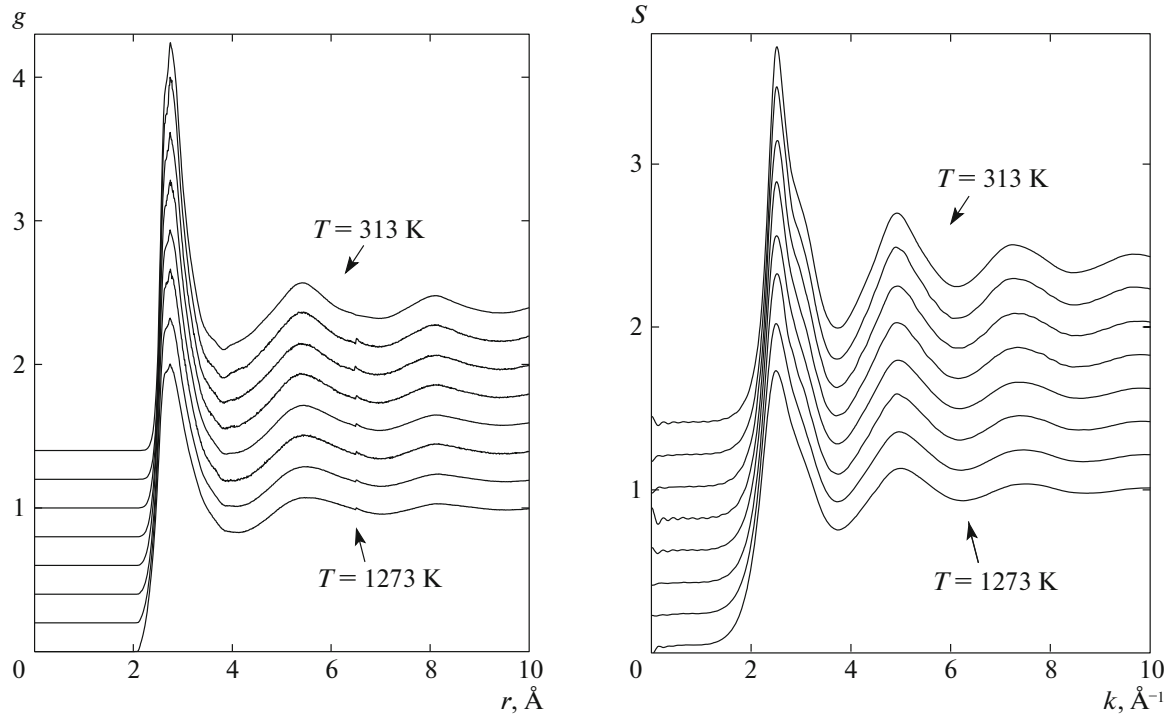

Fig. 1. Structural characteristics of liquid gallium at various temperatures, obtained from the atomic-dynamics simulation data. Radial distribution function (left) and static structure factor (right). The values on the ordinate axis correspond to the curves for the system at temperature $T = 1273$; the remaining curves are displaced upwards with a step of 0.2.

upon a further increase in wavenumber k. In spite of apparent similarity in the dependences of quantities $S(k)$ and $g(r)$ on k and r, it is quite difficult to establish an exact correlation between their individual characteristics, which is important for interpreting the measured structure factor $S(k)$.

In simple one-component liquids, the interaction between particles is described by spherical potential $U(r)$ with minimum $U(r_0)$, the position of which determines the correlation length comparable with the effective size (double radius) of particles, $r_1 = r_0$ [8]. The radial distribution function and the static structure factor of such a liquid at densities exceeding the density of the corresponding supercritical fluid can be characterized by a number of empirical peculiarities.

(i) The shape of function $g(r)$ is quite successfully reproduced by the linear combination of Gaussian functions with the number corresponding to the number of peaks [8] (see p. 144):

$$g(r) = \sum_i g_i(r), \quad i = 1, 2, \ldots, \tag{4}$$

where

$$g_i(r) = \frac{n_i}{\sqrt{2\pi\overline{\xi}_i^2}} \exp\left(-\frac{(r - r_i)^2}{2\overline{\xi}_i^2}\right). \tag{5}$$

Here, n_i is the effective ith coordination number, quantity $\overline{\xi}_i^2$ determines the peak width, and parameter r_i characterizes the position of the peak and, hence, the effective size of the ith coordination sphere.

(ii) If we define the distance between adjacent peaks in $g(r)$ in terms of $(r_{i+1} - r_i)$, where $i = 1, 2, 3$, and estimate the mean value as

$$\overline{\Delta r} = \frac{1}{3}\sum_{i=1}^{3}(r_{i+1} - r_i), \quad i = 1, 2, \ldots, \tag{6}$$

the value of $2\pi/\overline{\Delta r}$ approaches the value of the wavenumber characterizing the position of the principal peak in static structure factor $S(k_m)$; i.e.,

$$k_m \approx 2\pi/\overline{\Delta r}. \tag{7}$$

(iii) In set $[r_1, (r_2 - r_1), (r_3 - r_2), \ldots]$, the value of quantity r_1 characterizing the size of the first coordination sphere is maximal. In this case, the following empirical rule[1] holds:

$$\frac{r_1}{r_2 - r_1} \geq 1.1. \tag{8}$$

[1] From the results obtained in [46], we can state that in the case of a perfect crystal, expression (8) is transformed into an equality with values $r_1/(r_2 - r_1) = 2.42$ for the fcc, hcp, and sc lattices, $r_1/(r_2 - r_1) = 6.7$ for bcc lattice, and $r_1/(r_2 - r_1) = 1.89$ for a tetrahedral lattice.

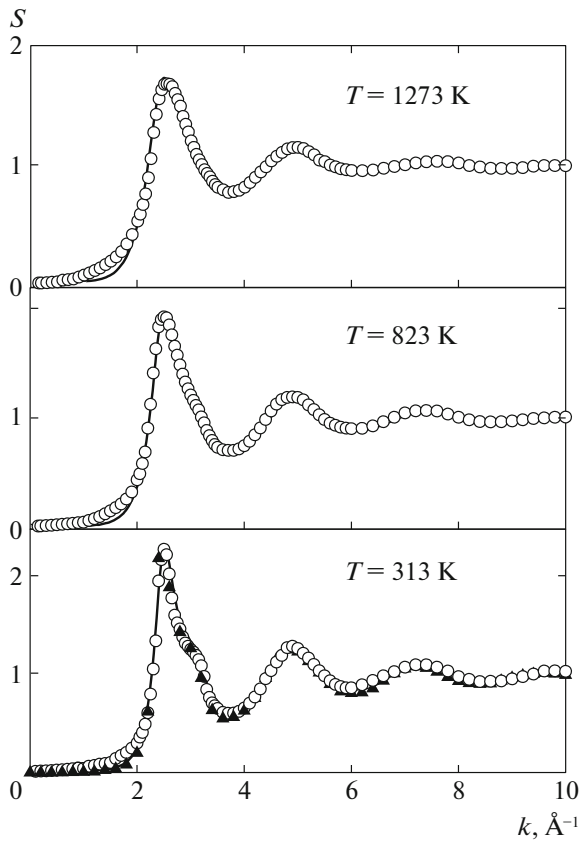

Fig. 2. Static structure factor of liquid gallium at various temperatures. The solid curve represents the results of simulation; circles correspond to X-ray scattering data [49]; triangles are experimental data on neutron diffraction for the system at $T = 313$ K [6].

(iv) According to another empirical Hansen–Verlet rule [47], the height of the principal peak in static structure factor $S(k_m)$ of a simple solidifying liquid exceeds 2.85, while in the case of an equilibrium fluid, we have $S(k_m) < 2.85$.

(v) The ratio of the radial distribution functions at the first minimum, $g(r_{\min})$, and at the first maximum, $g(r_1)$, is determined by the Wendt–Abraham parameter [48]

$$r^{WA} = g(r_{\min})/g(r_1).$$

The temperature dependence of parameter $r^{WA}(T)$ in the region containing the liquid–solid transition consists of two linear segments intersecting at the transition point with critical temperature T_c. As a rule, the Wendt–Abraham parameter is used for estimating the temperature of transition of a supercooled liquid into glass [23].

It is convenient to perform detailed analysis of local structural properties of liquid gallium by comparing the above-mentioned peculiarities in the structural characteristics with those for simple liquids. Figure 1 shows the radial distribution functions $g(r)$ and static structure factor $S(k)$ for particles in liquid gallium at various temperatures from interval $T \in$ [313 K; 1273 K], calculated from the results of atomic dynamics simulation. The radial distribution function was defined as

$$g(r) = \frac{V}{4\pi r^2 N}\left\langle \sum_{i=1}^{N} \frac{\Delta n_i(r)}{\Delta n} \right\rangle, \qquad (9)$$

and static structure factor $S(k)$ was defined by relation (3). Here, V is the volume of the simulation cell; quantity $\Delta n_j(r)$ determines the number of particles in a spherical layer of thickness Δr, separated by distance r from the ith particle; and angle brackets $\langle ... \rangle$ denote averaging over all particles of the system.

Curves $g(r)$ and $S(k)$ in Fig. 1, which were calculated for liquid gallium, resemble those for simple fluids. In this case, the clearly manifested peak in $g(r)$ (in $S(k)$) changes to rapidly damped oscillations with increasing r (wavenumber k). Further, the height of the principal peak in the static structure factor changes from $S(k_m) = 1.73$ at $T = 1273$ K to $S(k_m) = 2.3$ at $T = 313$ K, indicating fulfillment of the Hansen–Verlet rule according to which $S(k_m) < 2.85$ for a simple fluid. Nevertheless, the structural characteristics for liquid gallium exhibit considerable differences as compared to simple fluids. For example, the estimated value of the Wendt–Abraham parameter exhibits a nonlinear (in contrast to that in simple fluids) temperature dependence. The parameter changes from $r^{WA} = 0.202$ at $T = 313$ K to $r^{WA} = 0.414$ at $T = 1273$ K. Further, as can be seen from Fig. 1, the first peak in the radial distribution function $g(r)$ exhibits a clearly manifested asymmetry: the right wing of this peak is much more gently sloping than the left wing. Analogous asymmetry is also observed in the principal peak of static structure factor $S(k)$. Upon a decrease in temperature, the right-hand side of the principal peak of static structure factor $S(k)$ acquires a characteristic shoulder upon cooling in the range 2.8 Å$^{-1} \leqslant k \leqslant$ 3.1 Å^{-1} (see Fig. 2).

Positions of peaks r_i in the radial distribution function $g(r)$ for liquid gallium at $T = 313$ K and the values of parameters obtained by fitting expressions (4) and (5) to experimental data on $g(r)$. Subscript i indicates the serial number of the peak ($i = 1$, 2, 3, and 4). Remark: The first peak (for $i = 1$) in radial distribution function $g(r)$ is reproduced by a combination of three Gaussians of type (5).

i	1			2	3	4
r_i, Å	2.749			5.41	8.09	10.09
$r_i^{(g)}$, Å	2.72	3.0	3.6	5.30	8.0	10.61
$\overline{\xi}_i^2$, Å^2	0.02	0.06	0.14	1.0	1.3	1.35
n_i	0.73	0.75	0.39	2.75	2.8	2.43

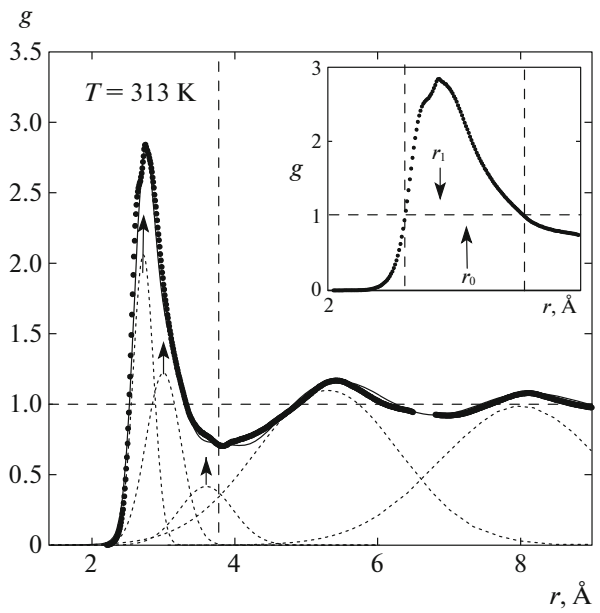

Fig. 3. Radial distribution function for atoms in liquid gallium at temperature $T = 313$ K: symbols represent the experimental data on X-ray diffraction [49]; the solid curve shows the results of fitting of expressions (4) and (5); dotted curves show individual contributions defined by expression (5). The inset shows the radial distribution function, where $r_1 = 2.749$ Å corresponds to the actual position of the tip of the first peak in $g(r)$; the value of $r_0 = 2.93$ Å indicates the position of the half-width of the first peak for the section at $g(r) = 1$.

Fitting of expressions (4) and (5) to experimental data on radial distribution function $g(r)$ shows that admissible agreement can be reached in the case when the first peak of $g(r)$ is reproduced at least by a combination of three Gaussian functions. At the same time, higher-order peaks in $g(r)$ ($i = 2, 3, ...$) for liquid gallium are reproduced by individual Gaussians of form (5). By way of example, Fig. 3 shows function $g(r)$ for liquid gallium at a temperature of $T = 313$ K, calculated from the results of simulation and fitting. The values of parameters appearing in expression (5) and obtained as a result of fitting for the given case are given in the table. Although the set of values presented in the table is not unambiguous for a correct reproduction of the shape of $g(r)$ with a preset accuracy (analogous agreement can be obtained with other parameter values), the results of fitting nevertheless indicate that the first coordination sphere is characterized not by a single correlation length as for simple fluids, but by a certain range of wavelengths. For example, in the case in Fig. 3, the range of correlation lengths should apparently include the values $r_1 = 2.72$ and 3.0 Å, while the third contribution with characteristic correlation length $r = 3.6$ Å comparable with the position of the first peak in $g(r)$ takes into account the correction for the uniform distribution of atoms at distances $r > r_1$, which is typical of fluids. Remarkably, such a wide spread in the correlation lengths characterizing the mutual arrangement of neighboring particles within the first coordination sphere, which is estimated as $r_{max}/r_{min} = 3.0/2.72 = 1.103$, is also observed in crystalline gallium. Namely, the Ga I stable crystalline phase under normal conditions forms a base-centered orthorhombic structure in such a way that the nearest neighbors are arranged at distances of 2.46, 2.70, 2.73, and 2.79 Å [3]. This set of values has a spread of $r_{max}/r_{min} = 2.79/2.46 = 1.134$, which is quite comparable with the estimated value of 1.103 for gallium in the liquid phase at temperature $T = 313$ K.

The positions of the first four peaks in radial distribution function $g(r)$ give, in accordance with expression (6), $\overline{\Delta r} \approx 2.64$ Å, where we choose for distance $r_1 = 2.749$ Å the position of the tip of the first peak in $g(r)$ (see Fig. 3). Here, wavenumber k_m is estimated as $2\pi/\overline{\Delta r} \approx 2.38$ Å^{-1}, which is smaller than the value of $k_m \approx 2.5$ Å^{-1}, indicating the position of the principal peak in static structure factor $S(k)$. This differs from the situation observed for simple fluids.

Further, in the case of liquid gallium, the relations between the characteristics of the first and second coordination spheres defined by inequality (8) is violated. For example, from the radial distribution of particles in liquid gallium at $T = 313$ K, we obtain $r_1/(r_2 - r_1) = 1.03$. Consequently, the size of the second coordination sphere is approximately equal to the doubled size of the first coordination sphere, which is unusual for a bulk condensed phase.

Liquid gallium cannot be attributed to the class of simple fluids mainly because the interaction of atoms in it cannot be reproduced by a spherical potential. The interaction between particles in liquid gallium generates configurations in which the arrangement of even the nearest neighbors (within the first coordination sphere) is characterized by a certain range of correlation lengths. In this case, the formation of such pairs of particles is "allowed," which in the model simple fluid corresponding to liquid gallium must be very close to each other or even coalesce. This can be shown by simple analysis of the radial distribution. For example, the first $g(r)$ peak in a simple fluid is almost symmetric in the upper half-plane defined by values of $g(r) \geqslant 1$; consequently, the tip lies at the middle of the peak (i.e., $r_0 \approx r_1$). As can be seen from the inset to Fig. 3, the tip of the peak for liquid gallium is displaced to the region of small r (namely, $r_1 < r_0$). In the case of a simple fluid corresponding to liquid gallium, it is precisely r_0 from these two characteristic lengths that could determine the equilibrium interparticle distance. This can be verified by substituting the value of r_0 for r_1 and verifying the above empirical rules. Fulfillment of relation (5) for the first peak on $g(r)$ with $r_0 \to r_1$ is obvious. Further, for $r_0 \to r_1$, we obtain from relation (6) $\overline{\Delta r} \approx 2.58$ Å and $k_m = 2\pi/\overline{\Delta r} = 2.43$ Å^{-1},

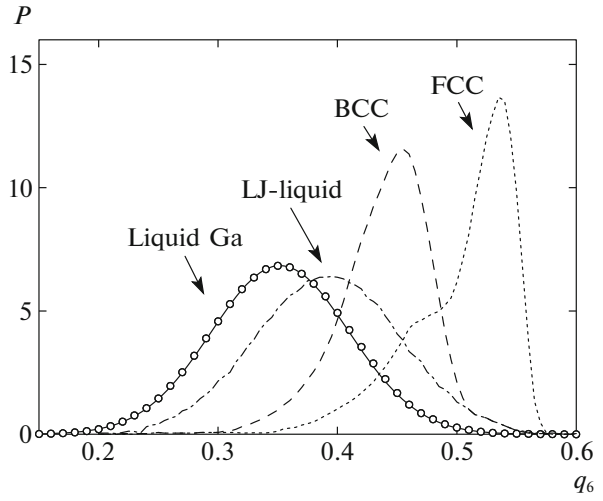

Fig. 4. Distribution over the values of local orientational order parameter $P[q_6(i)]$ for liquid gallium at $T = 313$ K: circles are the results of cluster analysis with simulation data; the solid curve is fitting of the distribution of type (12) and for a perfect crystal with the fcc lattice (dotted curve), bcc lattice (dashed curve), an equilibrium Lennard-Jones (LJ) liquid (dot-and-dash curve) based on the data from [50].

which approaches the actual position of the peak in the structure factor: $k_m \approx 2.5$ Å^{-1}. Finally, for inequality (8), we also obtain a confirmation: $r_0/(r_2 - r_1) \geqslant 1.1$.

Thus, the formation of the shoulder in the right part of the principal peak of static structure factor $S(k)$ in the range 2.8 Å$^{-1} \leqslant k \leqslant 3.1$ Å^{-1} at $T = 313$ K (see Fig. 2) can be explained by the predominance of correlations with characteristic lengths of 2.5 and 2.65 Å, which determine in $g(r)$ the mean distance $\overline{\Delta r}$ between the peaks and shift of the tip of the principal peak of static structure factor $S(k)$ to the left of the center.

4.2. Results of Cluster Analysis: Local Structural Properties

The quasi-solid-state interpretation of structural and dynamic properties of fluids [8] is usually constructed in analogy with similar properties in crystals. In such an interpretation, the existence of ordered regions (e.g., local crystalline domain-clusters and crystallites) is presumed as a rule, or a fluid is treated as a macroscopic crystalline phase characterized by excess defects and exhibiting elastic properties along with viscous properties. Taking into account the fact that structural peculiarities in the gallium melt considered here become well-pronounced at temperatures close to the melting point, it is expedient to assume that these features can be partly due to the presence of crystalline clusters in the melt. Analogous considerations were formulated in [9]. The results of atomic dynamics simulation, which agree with the experimental structural characteristic (static structure factor; see Fig. 2), enabled us to verify the assumption about the existence of ordered local atomic groups in the gallium melt. For this purpose, it is convenient to use the cluster analysis proposed by Wolde and Frenkel [50] and based on computation of the local orientational order parameters for each ith particle [51]:

$$q_6(i) = \left(\frac{4\pi}{13} \sum_{m=-6}^{6} \left| \frac{1}{N_b(i)} \sum_{j=1}^{N_b(i)} Y_{6m}(\theta_{ij}, \varphi_{ij}) \right|^2 \right)^{1/2}, \quad (10)$$

where $i = 1, 2, ..., N$ is the index of the particle in question; j is the index of a neighboring particle (i.e., a particle located in the first coordination sphere); $N_b(i)$ is the number of neighbors of the ith particle; $Y_{6m}(\theta_{ij}, \varphi_{ij})$ are the spherical harmonics; and θ_{ij} and φ_{ij} are the polar and azimuthal angles formed by radius vector $\mathbf{r}_{ij}$ in the coordinate system.

The form of the distribution over the angles of local order parameter $P[q_6(i)]$ depends on the type of the system. For example, in the case of a one-component liquid, the distribution is symmetric and has a maximum in the range $q_6 \leqslant 0.4$; for a perfect crystal with an fcc lattice, the peak of the distribution lies in the region of $q_6 = [0.45; 0.46]$; in the case of a perfect bcc lattice, the distribution peak is in the region of higher values: $q_6 = [0.52; 0.55]$.

The global orientational order parameter characterizing the degree of orientational ordering in the entire system can be defined as [52]

$$Q_6 = \left(\frac{4\pi}{13} \sum_{m=-6}^{6} \left| \frac{\sum_{i=1}^{N} \sum_{j=1}^{N_b(i)} Y_{6m}(\theta_{ij}, \varphi_{ij})}{\sum_{i=1}^{N} N_b(i)} \right|^2 \right)^{1/2}. \quad (11)$$

In the case of a disordered system, we have $Q_6 \to 0$, while for perfect crystalline structures, we obtain the following values: $Q_6^{(\mathrm{fcc})} = 0.5745$; for base-centered cubic lattice $Q_6 = 0.5106$; $Q_6^{(\mathrm{bcc})} = 0.3536$, $Q_6^{(\mathrm{hcp})} = 0.4848$, etc. [52].

The results of cluster analysis based on the atomic dynamics simulation of liquid gallium did not confirm the presence of local atomic groups in the system at temperatures of $T \in$ [313 K; 1273 K], which could be attributed to crystalline clusters. For example, the calculated orientational order parameter Q_6 in this temperature interval assumes values of $Q_6 = 0.005 \pm 0.002$, indicating a high degree of disorder in the system, which is typical of an equilibrium fluid.

In Fig. 4, the calculated distribution over the values of local order parameter $P(q_6)$ for liquid gallium at a temperature of $T = 313$ K is compared for better visualization with the distributions for a Lennard-Jones fluid and for crystal phases with fcc and bcc lattices. It

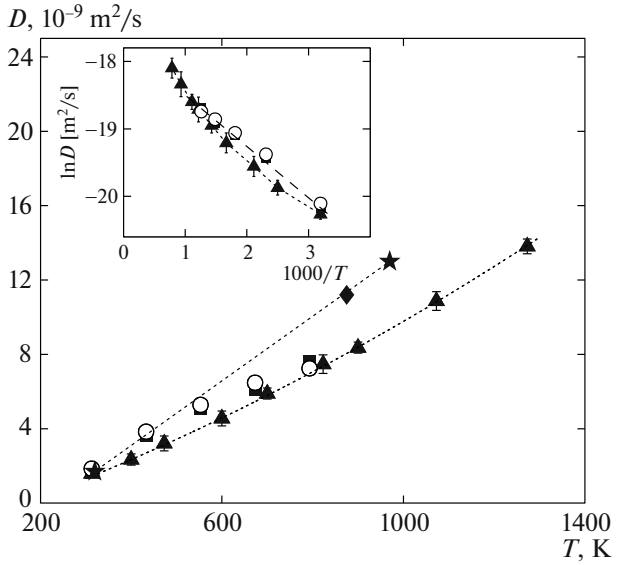

Fig. 5. Temperature dependence of self-diffusion coefficient $D(T)$ for gallium melt: dark triangles are the results of atomic dynamics simulation; circles and squares are experimental results of coherent and incoherent neutron scattering in liquid gallium [34]; the diamond is the experimental result [31]; stars are the results of molecular-dynamics calculations [30]. The dashed straight line in the inset is the result of fitting of expression (13) to experimental values.

can be seen that in the case of liquid gallium, the $P(q_6)$ distribution is symmetric and has a shape corresponding to the distribution for the Lennard–Jones fluid. Moreover, the $P(q_6)$ distribution for liquid gallium is correctly reproduced by the dependence

$$P(q_6) = A\exp[-C(q_6 - q_6^{\max})^2], \tag{12}$$

where $A = 6.84$, $C = 150$, and $q_6^{\max} = 0.352$. Thus, the distribution peak located at point $q_6^{\max} = 0.352$ is shifted to the range of lower values as compared to the Lennard–Jones fluid, for which $q_6^{\max} = 0.395$. This means that liquid gallium (even at $T = 313$ K, i.e., near the melting point) is a homogeneous disordered system in which there are apparently no stable localized ordered structures.

5. SELF-DIFFUSION OF LIQUID GALLIUM

The self-diffusion coefficient can be determined from the atomic dynamics simulation data the using the Einstein relation [53]

$$D = \lim_{t\to\infty}\frac{\langle|\Delta\mathbf{r}(t)|^2\rangle}{6t}, \tag{13}$$

where

$$\langle|\Delta\mathbf{r}(t)|^2\rangle = \frac{1}{N}\left\langle\sum_{j=1}^{N}|\mathbf{r}_j(t) - \mathbf{r}_j(0)|^2\right\rangle \tag{14}$$

is the mean-squared displacement; angle brackets $\langle ...\rangle$ indicate averaging over the particle ensemble. In Fig. 5, the values of the self-diffusion coefficient for liquid gallium, calculated for the temperature range $T \in$ [313 K; 1273 K] from the molecular dynamics results with the AEM potential are compared with experimental neutron scattering data [34]. It can be seen that the results of atomic dynamics simulation agree well with the experimental data. The values of the self-diffusion coefficient D at temperatures of $T =$ 313 K and $T \sim 790$ K are almost identical to the experimental data; however, in the intermediate temperature interval from 350 to 730 K, insignificant differences are observed. The temperature dependence of the self-diffusion coefficient shown in the inset to Fig. 5 on the logarithmic scale shows that the scattering data fit into a straight line and, hence, are reproduced by the well-known expression of the form [8]

$$D = D_0\exp(-E_a/k_BT). \tag{15}$$

From the experimental dependence, we obtain activation energy $E_a = 1.01 \times 10^{-20}$ J and pre-exponential factor $D_0 = 1.87 \times 10^{-8}$ m^2/s. On the other hand, the simulation results indicate that self-diffusion in liquid gallium in the given temperature range is not reproduced by expression (15) with fixed values of E_a and D_0. Estimates give $E_a = 9.73 \times 10^{-21}$ J and $D_0 = 1.5 \times 10^{-8}$ m^2/s for the temperature interval $T \in$ [313 K; 600 K] and $E_a = 1.68 \times 10^{-20}$ J and $D_0 = 3.44 \times 10^{-8}$ m^2/s for the temperature range $T \in$ [600 K; 1273 K].

6. MICROSCOPIC COLLECTIVE AND SINGLE-PARTICLE DYNAMICS

The peculiarities of single-particle dynamics, as well as collective vibrational dynamics associated with propagation of acoustic-like waves in a many-particle system, are fully reflected in the spectral densities $\tilde{Z}(\omega)$ of autocorrelation function (ACF) of the particle velocity and of the time correlation function (TCF) of the longitudinal (L) and transverse (T) currents ($\tilde{C}_L(k, \omega)$ and $\tilde{C}_T(k, \omega)$, respectively). Here, quantity $\tilde{Z}(\omega)$ is defined as [54, 55]

$$\tilde{Z}(\omega) = \frac{2}{\pi}\int_0^\infty\frac{\langle\boldsymbol{\vartheta}(0)\boldsymbol{\vartheta}(t)\rangle}{\langle|\boldsymbol{\vartheta}|^2\rangle}e^{i\omega t}dt, \tag{16}$$

where $\langle|\vartheta|^2\rangle = 3k_BT/m$ is the rms velocity of a particle of mass m. It should be noted that spectral density $\tilde{Z}(\omega)$ is identical to the reduced density of states associated with single-particle vibrational dynamics

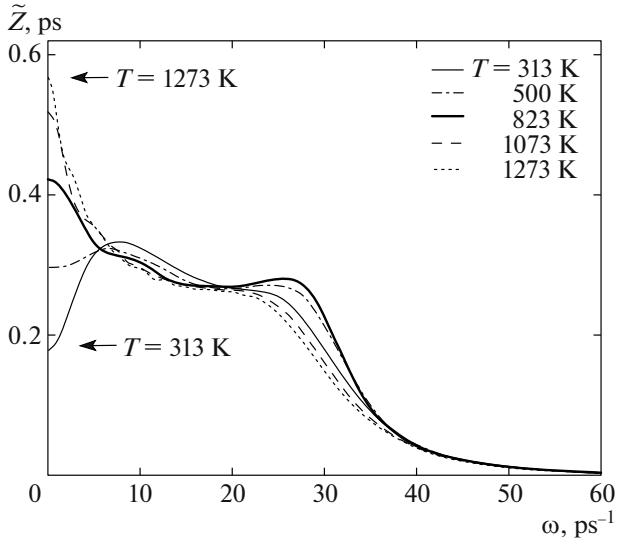

Fig. 6. Vibrational density of states of liquid gallium at temperatures T = 313, 500, 823, 1073, and 1273 K, calculated from the atomic dynamics simulation data.

(vibrational density of states) [53], for which the normalization condition has the form

$$\int_0^\infty \tilde{Z}(\omega)d\omega = 1.$$

The spectral densities of TCFs of the longitudinal and transverse currents can be defined as [56]

$$\tilde{C}_\alpha(k,\omega) = \frac{1}{t_M}\left|\int_0^{t_M} j_\alpha(k,t)e^{i\omega t}dt\right|^2, \quad \alpha = \{L,T\}, \quad (17)$$

where

$$j_L(k,t) = \frac{1}{\sqrt{N}}\sum_l^N \left(\mathbf{e}_k, \boldsymbol{\vartheta}_l(t)\right)e^{-i(\mathbf{k},\mathbf{r}_l(t))} \quad (18)$$

is a dynamic variable corresponding to the longitudinal current and

$$j_T(k,t) = \frac{1}{\sqrt{N}}\sum_l^N \left[\mathbf{e}_k, \boldsymbol{\vartheta}_l(t)\right]e^{-i(\mathbf{k},\mathbf{r}_l(t))} \quad (19)$$

is a dynamic variable characterizing the transverse current. The parentheses $(\cdot, \cdot)$ and brackets $[\cdot, \cdot]$ in expressions (18) and (19) indicate the scalar and vector products, respectively; quantities $\mathbf{r}_l(t)$ and $\boldsymbol{\vartheta}_l(t)$ define the radius vector and velocity of the lth atom at instant t; $\mathbf{e}_k$ is the unit vector codirectional with wavevector $\mathbf{k}$; and t_M is the time scale over which the evolution of the system is traced.

In contrast, spectral densities $\tilde{Z}(\omega)$ and $\tilde{C}_L(k, \omega)$ are directly related to the quantities measured in experiments on inelastic scattering of neutrons, viz., the dynamic structure factor

$$S(k,\omega) = \frac{1}{2\pi N}\int_{-\infty}^{\infty} dt e^{-i\omega t}\sum_{l,j}\langle e^{-i\mathbf{k}\cdot\mathbf{r}_l(0)}e^{i\mathbf{k}\cdot\mathbf{r}_j(t)}\rangle \quad (20)$$

and the incoherent scattering function

$$S_s(k,\omega) = \frac{1}{2\pi N}\int_{-\infty}^{\infty} dt e^{-i\omega t}\sum_{j}\langle e^{-i\mathbf{k}\cdot\mathbf{r}_j(0)}e^{i\mathbf{k}\cdot\mathbf{r}_j(t)}\rangle. \quad (21)$$

For example, for the pair of quantities $\tilde{Z}(\omega)$ and $S_s(k, \omega)$, we can write in the long-wavelength limit [53]

$$\tilde{Z}(\omega) = \omega^2 \lim_{k\to 0}\frac{S_s(k,\omega)}{k^2}, \quad (22)$$

while expressions (17), (18), and (20) give

$$\tilde{C}_L(k,\omega) = \frac{\omega^2}{k^2}S(k,\omega). \quad (23)$$

The vibrational density of states of liquid gallium calculated for some temperatures on the basis of atomic dynamics simulation data are shown in Fig. 6. It can be seen that in the given temperature range $T \in$ [313 K; 1273 K], the spectral curves demonstrate clearly manifested differences only at frequencies $\omega <$ 7 ps^{-1} and 20 ps$^{-1} < \omega <$ 35 ps^{-1}. Component $\tilde{Z}(\omega_a)$ of the vibrational density of states at a certain nonzero frequency $\omega_a \neq 0$ characterizes the contribution of the vibrational process with corresponding frequency ω_a, while intensity $\tilde{Z}(\omega = 0)$ (at zero frequency) characterizes self-diffusion, which follows directly from the Kubo–Green relation

$$D = \frac{k_B T}{m}\int_0^\infty \frac{\langle \boldsymbol{\vartheta}(0)\boldsymbol{\vartheta}(t)\rangle}{\langle|\boldsymbol{\vartheta}|^2\rangle}dt = \frac{\pi}{2}\frac{k_B T}{m}\lim_{\omega\to 0}\tilde{Z}(\omega). \quad (24)$$

In other words, the larger value of $\tilde{Z}(0)$ corresponds to the larger value of self-diffusion coefficient D. As can be seen from Fig. 6, the value of $\tilde{Z}(0)$ decreases with temperature, which fully agrees with the results on the temperature dependence of the self-diffusion coefficient (see Section 5). Further, for relatively high temperatures $T \geqslant 600$ K, the peak of $\tilde{Z}(\omega)$ corresponds to zero frequency, indicating the leading role of the diffusion regime in the single-particle dynamics as compared to the vibrational degrees of freedom. As the temperature decreases to $T \geqslant 600$ K, the vibrational density of states $\tilde{Z}(\omega)$ acquires clearly manifested peaks corresponding to frequencies $\omega \sim 8 \pm 1$ ps^{-1} and $\omega \sim 28 \pm 2$ ps^{-1}. In the low-temperature region $T \leqslant 600$ K, the intensities of these high-frequency components of $\tilde{Z}(\omega)$ exceed the value of $\tilde{Z}(\omega = 0)$, which may indicate that the leading role in the single-particle dynamics is now played by the

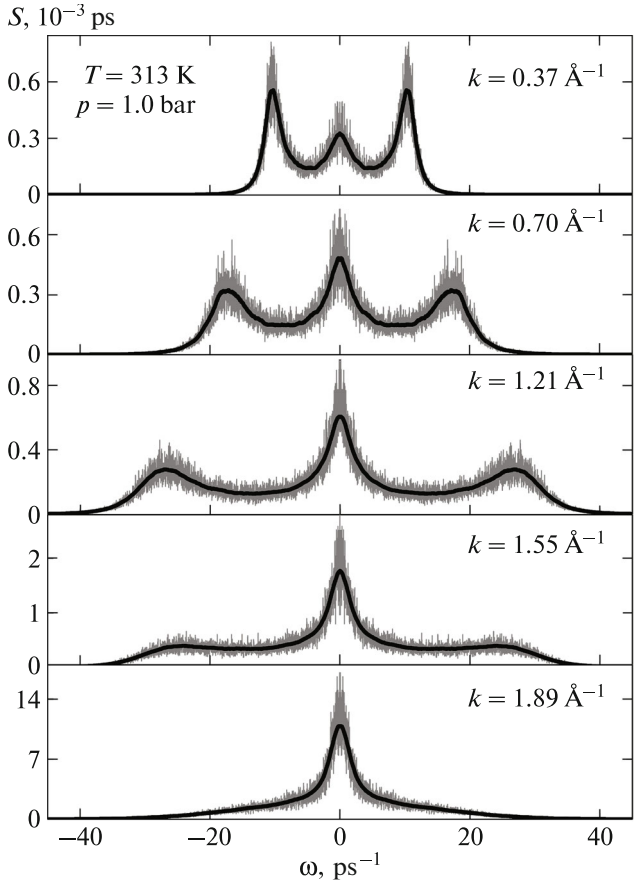

Fig. 7. Spectra of the dynamic structure factor of liquid gallium at temperature $T = 313$ K for various values of wavenumber k.

vibration and not diffusion regime. It should be recalled that in fitting of $D(T)$ by Arrhenius dependence (15), it is precisely the value of $T \approx 600$ K that corresponds to the transition temperature at which parameters D_0 and E_a change (see Section 5).

The existing methods for identifying a conditional transition of a fluid from a regime in which solidlike features prevail to a regime with a gaslike behavior in the microscopic dynamics were analyzed in detail in [57]. As the criterion, quantity R was proposed, defined as the ratio of the time scales of the diffusion and vibrational processes. The line on the phase diagram corresponding to this transition with the value of criterion $R = 1$ was denoted in [57] as the Frenkel line. As a development of the idea put forth in [57], we can propose the numerical estimation of the time scales of the diffusion and vibrational processes in terms of the height of the zeroth component in the vibrational density of states $\tilde{Z}(0)$ and the high-frequency peak (or arm) $\tilde{Z}(\omega \neq 0)$, i.e.,

$$R = \frac{\tilde{Z}(0)}{\tilde{Z}(\omega \neq 0)}. \qquad (25)$$

Figure 7 shows the spectra of dynamic structure factor $S(k, \omega)$ calculated from the atomic dynamics simulation data for liquid gallium at $T = 313$ K and for various values of wavenumber k. It should be noted that wavenumber $k_m = 2.5$ Å^{-1} at this temperature determines the position of the principal peak in static structure factor $S(k)$ (see Fig. 2), while a value of $k_m/2 = 1.25$ Å^{-1} gives an estimate for the boundary of the pseudo-Brillouin zone. In the $S(k, \omega)$ spectra in the range of wavenumbers from small values to $k \approx 2k_m/3$, the three-peak structure is clearly manifested with a central peak (at $\omega = 0$) and the high-frequency symmetric doublet (with characteristic frequencies $\pm\omega_c \neq 0$). Since the high-frequency peaks in $S(k, \omega)$ are associated with acoustic excitations, their positions in the spectra at fixed k can be used to construct approximate dispersion curves $\omega_c(k)$. It should therefore be noted that the actual (and not approximate) dispersion dependences correspond to the peaks in the spectral densities $\tilde{C}_L(k, \omega)$ and $\tilde{C}_T(k, \omega)$ of the longitudinal and transverse currents [58].[2]

Figure 8 shows the spectral densities $\tilde{C}_L(k, \omega)$ and $\tilde{C}_T(k, \omega)$ calculated for liquid gallium at $T = 313$ K from the simulation data. The spectra of both quantities characterizing the collective dynamics with longitudinal and transverse polarizations contain high-frequency peaks. The position of the peak in $\tilde{C}_L(k, \omega)$ indeed almost coincides with the position of the inelastic component of dynamic structure factor $S(k, \omega)$, while the position of the peak in the TCF spectral density $\tilde{C}_T(k, \omega)$ of the transverse current is characterized by lower values (at fixed and identical values of k). This can clearly be seen from the dispersion curves of acoustic vibrations with longitudinal and transverse polarizations, calculated from spectral densities $\tilde{C}_L(k, \omega)$ and $\tilde{C}_T(k, \omega)$ shown in Fig. 9. In the range of small values of the wavenumber ($k \leqslant 0.8$ Å^{-1}), dispersion curves $\omega_c^L(k)$ and $\omega_c^T(k)$ are close to linear dependences with slopes that can be used to estimate the velocities of sound $\vartheta_L = 2523$ m/s and $\vartheta_T = 798$ m/s. The upper dispersion curves originate from zero wavenumber k, while the lower dispersion branch is absent in the interval $0 < k \leqslant 0.25$ Å^{-1}: the peak in the $\tilde{C}_T(k, \omega)$) spectrum for this range of k values lies exactly at the zero frequency. Further, the peak in the $\tilde{C}_T(k, \omega)$ spectrum is shifted towards nonzero frequencies only for $k > 0.25$ Å^{-1}. Such a behavior in the dispersion branch $\omega_c^T(k)$ is due to the absence of the elastic response of the system on spatial scales exceeding $l = (2\pi/0.25\ \text{Å}^{-1}) \approx 25$ Å.

[2] It can be seen from expression (23) that dynamic structure factor $S(k, \omega)$ is directly related to thr quantity $\tilde{C}_L(k, \omega)$. The conditions for the existence of peaks in these quantities are different, although they can lead to close results.

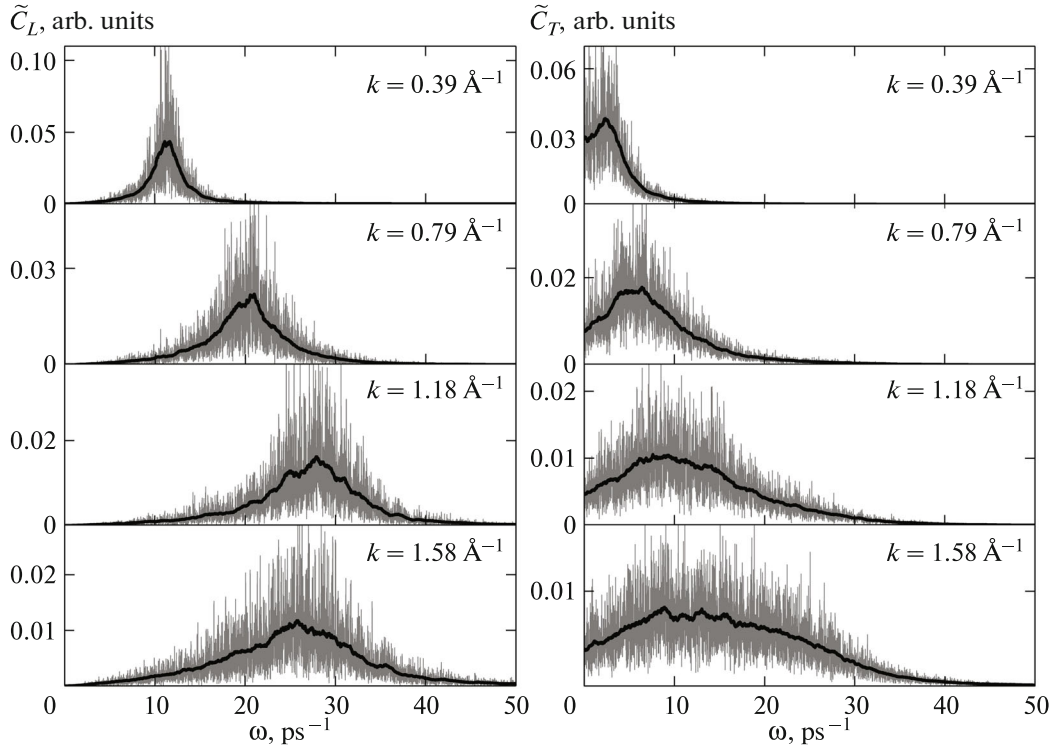

Fig. 8. Spectral densities of the TCF of longitudinal current $\tilde{C}_L(k, \omega)$ (left part) and transverse current $\tilde{C}_T(k, \omega)$ (right part) for liquid gallium at temperature $T = 313$ K for various values of wavenumber k.

The dispersion curves resemble acoustic dispersion branches for crystals: with increasing k, frequencies $\omega_c^{L,T}$ first increase, attain their maximal values, and then exhibit a decrease. Remarkably, the peaks on the dispersion curves lie outside the first pseudo-Brillouin zone with the boundary at 1.25 Å^{-1} at this temperature and lie at $k \approx 1.45 \pm 0.03$ Å^{-1}, which corresponds to the Debye wavenumber $k_D = (6\pi^2 N/V)^{1/3} = 1.46$ Å^{-1}. As can be seen from Fig. 9, the results of atomic dynamics calculations for the dispersion curves agree well with the inelastic neutron scattering data, with the results of quantum-mechanical simulation [32], and with experimental data on inelastic scattering of X-rays [32], where the values of $\omega_c^T(k)$ (two points for the "T-mode" in the figure) were estimated from singularities in the shape of the experimental spectra of the dynamic structure factor.

It is important to note that the dispersion dependences clarify the interpretation of the form of the vibrational density of states $\tilde{Z}(\omega)$. As shown above (see Fig. 6), spectral density $\tilde{Z}(\omega)$ for liquid gallium at $T = 313$ K has a bimodal form. Comparison of the dispersion curves $\omega_c^{L,T}(k)$ and spectral density $\tilde{Z}(\omega)$ in Fig. 9 shows that the low-frequency peak in $\tilde{Z}(\omega)$ appears due to vibrational motion of particles, which contributes to the acoustic mode with the transverse polarization, while the singularity of the high-frequency peak in $\tilde{Z}(\omega)$ is associated with the vibrational motion of particles generating acoustic waves with the longitudinal polarization. On the other hand, quantity $\tilde{Z}(\omega)$ contains information about the processes associated with vibrational motion of particles over various lengths $l = 2\pi/k$ irrespective of the direction. Such considerations make it possible to represent quantity $\tilde{Z}(\omega)$ in the context of the generalized Debye model in the form [59]

$$\tilde{Z}(\omega) = \frac{2m}{k_B T k_D^3} \int_0^{k_D} k^2 [\tilde{C}_L(k, \omega) + 2\tilde{C}_T(k, \omega)] dk, \quad (26)$$

where k_D is the Debye wavenumber, N is the number of particles, and V is the system volume. On the basis of available spectra $\tilde{C}_L(k, \omega)$ and $\tilde{C}_T(k, \omega)$ of the longitudinal and transverse currents, integral relation (26) was evaluated numerically. Integration step Δk was 0.1 Å^{-1}; the lower integration limit was set at 0.1 Å^{-1}, and the upper limit was $k_D \approx 1.5$ Å^{-1}. The results of numerical calculation of expression (26) are shown in Fig. 10, where these results are compared with the value of $\tilde{Z}(\omega)$ obtained directly from atomic-dynamics calculations. It can be seen from the figure that expression (26) exactly reproduces all main features in the vibrational density of states $\tilde{Z}(\omega)$. This fully con-

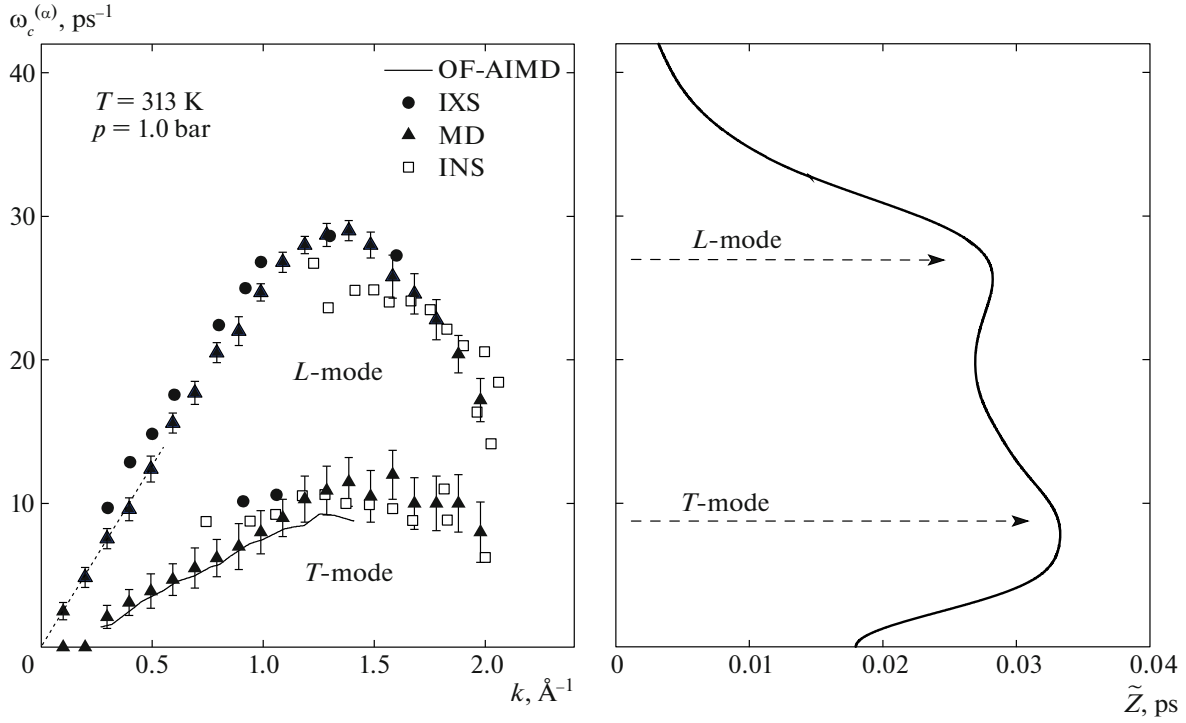

Fig. 9. (left) Dispersion of collective excitations $\omega_c^{(\alpha)}(k)$ of the longitudinal $\{\alpha \equiv L\}$ and transverse $\{\alpha \equiv T\}$ polarizations: triangles are the results of atomic dynamics simulation; squares are the results of interpretation of neutron inelastic scattering data; circles are experimental data on inelastic scattering of X-rays [32]; the solid curve is the estimate of the dispersion branch of transverse acoustic vibrations, obtained from the results of quantum-mechanical simulation [32]. The slopes of the interpolation (for the L mode) and extrapolation (for the T mode) straight lines to the range of small wavenumbers determine the corresponding sound velocities $\vartheta_L = 2523$ m/s and $\vartheta_T = 798$ m/s. (right) Spectral density of autocorrelation function of velocity $\tilde{Z}(\omega)$ of atoms in gallium melt at temperature $T = 313$ K.

firms the above conclusions that the form of $\tilde{Z}(\omega)$ is determined by the vibrational modes participating in the formation of acoustic waves with longitudinal and transverse polarizations. Expression (26) makes it possible to separate the estimates of individual contributions:

$$\tilde{Z}(\omega) = \tilde{Z}_L(\omega) + \tilde{Z}_T(\omega), \tag{27a}$$

$$\tilde{Z}_L(\omega) = \frac{2m}{k_B T k_D^3}\int_0^{k_D} k^2 \tilde{C}_L(k,\omega)dk, \tag{27b}$$

$$\tilde{Z}_T(\omega) = \frac{4m}{k_B T k_D^3}\int_0^{k_D} k^2 \tilde{C}_T(k,\omega)dk. \tag{27c}$$

It can be seen from Fig. 10 that the positions of the peaks in $\tilde{Z}_L(\omega)$ and $\tilde{Z}_T(\omega)$ correspond to the peaks in the initial $\tilde{Z}(\omega)$ spectrum. For example, the peak of the $\tilde{Z}_L(\omega)$ contribution corresponds to a frequency of about 28 ps^{-1}, while the $\tilde{Z}_T(\omega)$ peak lies at a frequency of about 8 ps^{-1}.

Further, expression (23) implies that

$$\lim_{\omega\to 0} \tilde{C}_L(k,0) = 0, \tag{28}$$

while integral expression (27b) gives

$$\lim_{\omega\to 0} \tilde{Z}_L(k,0) = 0. \tag{29}$$

Consequently, zero component $\tilde{Z}(0)$ of the vibrational density of states is determined only by quantity $\tilde{Z}_T(0)$, and Kubo–Green relation (24) for the self-diffusion coefficient can be written in the form

$$D = \frac{2\pi}{k_D^3}\int_0^{k_D} k^2 \tilde{C}_T(k,0)dk. \tag{30}$$

It will be shown below that this expression makes it possible to obtain the modified Einstein–Stokes relation. Further, from relations (27) and (29), we obtain

$$\tilde{Z}(0) = \frac{4m}{k_B T k_D^3}\int_0^{k_D} k^2 \tilde{C}_T(k,0)dk, \tag{31}$$

which clarifies the low-frequency behavior of quantity $\tilde{Z}(\omega)$ containing component $\tilde{Z}(\omega = 0)$ with nonzero

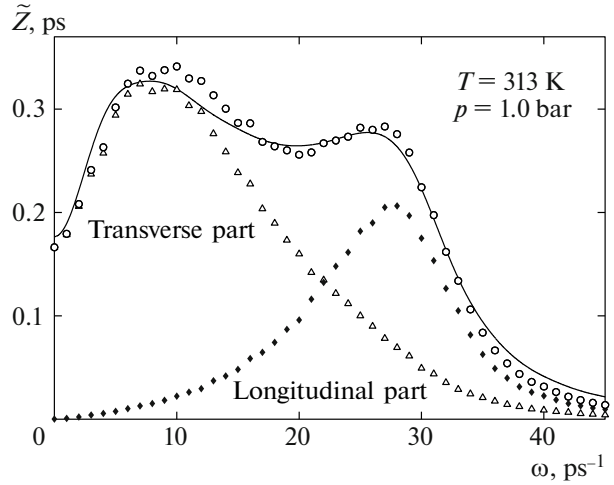

Fig. 10. Spectral density of autocorrelation function of velocity of particles in liquid gallium at $T = 313$ K: the solid curve represents the results of atomic dynamics computer simulation; circles are the results of theoretical calculations based on formula (26); diamonds and triangles correspond to the longitudinal and transverse contributions $\tilde{Z}_L(\omega)$ and $\tilde{Z}_T(\omega)$.

values, which is not observed for crystals. For example, it follows from expression (31) that the intensity of component $\tilde{Z}(\omega = 0)$ is formed by low-frequency vibrational processes taken into account by spectral density $\tilde{C}_T(k, \omega)$ in the range of wavenumbers $k \in [0; k_D]$. Thus, an increase in the intensity of component $\tilde{Z}(\omega = 0)$ with the melt temperature can be due to expansion of the range of wavenumbers k, where the peak in spectral density $\tilde{C}_T(k, \omega)$ corresponds to zero frequency. On dispersion curve $\omega_c^T(k)$, this is manifested as an increase upon heating in the range of wavenumbers (up to the long-wave limit) in which a dip is observed in dispersion (i.e., $\omega_c^T(k) = 0$; see Fig. 9).

In [60], a simplified method in which the $\tilde{Z}(\omega)$ contour is fitted by a set of Lorentzian functions was employed for interpreting the vibrational density of states $\tilde{Z}(\omega)$ of water molecules, calculated by molecular dynamics simulation with a certain model potential. It was assumed that the Lorentzian functions reproduce individual regimes (modes of vibrational dynamics of particles), and the number of these elementary functions is determined by the features of the initial $\tilde{Z}(\omega)$ spectrum (as a rule, maxima and broadenings the positions of which determine the shift of the Lorentzian functions along the ω axis, i.e., in frequency). In addition to the frequencies corresponding to a shift for each Lorentzian function, the height and halfwidth should be selected. Thus, in accordance with the method proposed in [60], reproduction of the $\tilde{Z}(\omega)$ spectrum containing, for example, q singularities requires $3q$ fitting parameters. In contrast to the method described in [60], the computation of the value of $\tilde{Z}(\omega)$ with the help of expression (26) does not require any fitting parameters, and the input quantities in this case are only spectral densities $\tilde{C}_L(\omega)$ and $\tilde{C}_T(\omega)$ defined in the half-interval of wavenumbers $0 < k \leqslant k_D$. It should also be noted that the forms of individual contributions $\tilde{C}_L(\omega)$ and $\tilde{C}_T(\omega)$ do not correspond to the Lorentzian functions (see Fig. 10).

7. MODIFIED EINSTEIN–STOKES RELATION

The relation between self-diffusion coefficient D and shear viscosity η for a fluid is defined by the Einstein–Stokes relation

$$D\eta = \frac{k_B T}{6\pi r_0}, \tag{32}$$

where r_0 is the radius of a spherical particle. In the case of simple fluids, relation (32) can be written in the form [61]

$$D\eta = \frac{k_B T}{\xi}\rho^{1/3}, \tag{33}$$

which includes number density $\rho = N/V$. Here, ξ is the mean number of the nearest neighbors lying in the same plane with the diffusing atom [62]: $\xi = 6$ for a close-packed system of atoms and $\xi = 5.6$ for a simple fluid.

On the other hand, the expression relating the self-diffusion coefficient and shear viscosity can be derived from expression (30). For small wavenumbers and frequencies corresponding to hydrodynamic conditions, spectral density $\tilde{C}_T(k, \omega)$ is reproduced by the relation [63–65]

$$\tilde{C}_T(k,\omega) = k_B T \frac{(\eta/\rho)k^2}{\pi[\omega^2 + (\eta/\rho)^2 k^4]}, \tag{34}$$

which yields

$$\tilde{C}_T(k,0) = \frac{1}{\pi}\frac{\rho k_B T}{\eta k^2}. \tag{35}$$

Assuming that this expression with the k-dependence of the form

$$\tilde{C}_T(k,0) \sim \frac{1}{k^2} \tag{36}$$

holds in the range of wavenumbers from $k \approx 0$ to k_D and taking into account expression (30), we obtain the Einstein–Stokes relation

$$D\eta = 2(6\pi^2)^{-2/3} k_B T \rho^{1/3}. \tag{37}$$

Comparing this expression with (33), we find that relation (37) gives too high a value for parameter ξ ($(1/2)(6\pi^2)^{2/3} \approx 7.6$). This can be explained by the results in Fig. 11. It can be seen that the proposed

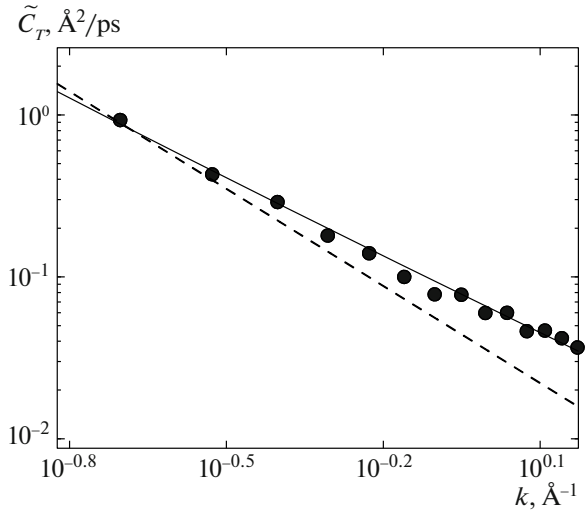

Fig. 11. Spectral component $\tilde{C}_T(k, \omega = 0)$ of liquid gallium at $T = 313$ K; circles are the results of atomic dynamics calculations; the dashed line is fitting by expression $\tilde{C}_T(k, 0) = 0.035k^{-2}$; solid line is fitting by expression $\tilde{C}_T(k, 0) = 0.055k^{-3/2} + 0.01k^{-2}$.

$(1/k^2)$ dependence in relation (35) is violated upon an increase in wavenumber k when the graph becomes more gently sloping. Instead of this, the behavior of quantity $\tilde{C}_T(k, 0)$ is quite correctly reproduced by the following relation:

$$\tilde{C}_T(k,0) = C_1 k^{-3/2} + C_2 k^{-2}, \qquad (38)$$

where $C_1, C_2 \geqslant 0$. With allowance for this relation, we then obtain from expression (30)

$$D = \frac{4\pi}{3} C_1 (6\pi^2 \rho)^{-1/2} + 2\pi C_2 (6\pi^2 \rho)^{-2/3}. \qquad (39)$$

8. CONCLUSIONS

The experimental data and the results of atomic dynamics simulation of liquid gallium make it possible to verify some of the above assumptions concerning its local structure by comparison with the structural properties of simple fluids and to obtain some results. For example, the results of cluster analysis carried out on the basis of simulation data indicate that liquid gallium at temperatures exceeding melting point T_m is a fluid containing no stable local crystalline formations. At the same time, the nearest neighbors of atoms in liquid gallium are characterized by a range of correlation lengths that can be estimated directly from the shape of the first peak of the radial distribution function. Analysis of the nearest surroundings forming the first coordination sphere indicates the presence in liquid gallium of dimers, viz., atomic pairs in which the distance between the atoms is smaller than 2.72 Å. Remarkably, the existence of such Ga_2 quasi-molecules with a bond of 2.46 Å was pointed out in [3] for crystalline gallium. These local structural features are responsible for the displacement (as compared to simple fluids) of the positions of the second, third, etc., peaks in the radial distribution function, which in turn determines the asymmetry and formation of an shoulder in the principal peak of the static structure factor. In this connection, ab initio calculations could be very useful for additional confirmation of the presence in liquid gallium of dimers with an ultrashort bond.

At present, information on the temperature dependence of the self-diffusion coefficient of liquid gallium is quite contradictory. For instance, in early publications on simulation [30] and neutron spectroscopy [31], the self-diffusion coefficient was given only for three temperatures ($T = 320$, 875, and 970 K). Nevertheless, as shown in [34], these values contradict the temperature dependence of the self-diffusion coefficient obtained on the basis of the results of later experiments on neutron scattering. The results of atomic dynamics simulation reported in this study confirm the conclusions drawn in [34] concerning the temperature dependence of the self-diffusion coefficient. In addition, fitting of the temperature dependence of the self-diffusion coefficient for liquid gallium by the Arrhenius equation indicates transition temperature $T \approx 600$ K. Analysis of the spectral density of the autocorrelation function of the particle velocity shows that the leading role in the single-particle dynamics passes from the vibrational to the diffusion mode at the same temperature.

Our results indicate the existence of two dispersion branches in the collective atomic dynamics of liquid gallium, which characterize the propagation of acoustic-like excitations with the longitudinal and transverse polarizations. We have observed convincing agreement between the experimental data on neutron scattering and the results of atomic dynamics simulation. It should therefore be noted that the "trace" of transverse vibrations is present in the experimental dynamic structure factor, which is a quantity that, according to definition, directly takes into account only the longitudinal collective dynamics. In addition, the results of simulation indicate that in the range of small values of the wavenumber, the dispersion curve associated with transverse vibrations is absent, which is not surprising since this indicates the absence of macroscopic elastic properties in the fluid. At the same time, quasi-elasticity, which is manifested in the formation of this dispersion curve only at finite values of the wavenumber (in the vicinity of the boundary of the first pseudo-Brillouin zone) is due to the interaction between particles. Consequently, it can be expected that with increasing temperature and far from the melting point, the range of wavenumbers in which this dispersion branch is not observed must increase.

The spectral densities of the correlation functions of the longitudinal and transverse currents obtained from the results of atomic dynamics simulation of liquid gallium in a wide range of wavenumbers have made it possible to calculate the vibrational density of states using the generalized Debye model. It was found that the bimodal nature of the vibrational density of states of liquid gallium at temperatures close to the melting point is determined by the vibrational single-particle dynamics contributing to the formation of acoustic-like collective excitations with longitudinal and transverse polarizations. The generalized Debye model makes it possible to take into account and separate these two contributions. We have derived the expression for the self-diffusion coefficient containing low-frequency components of the spectral density of the transverse current for a range of wavenumbers, as well as the Debye wavenumber.

Finally, we have obtained modified Einstein–Stokes expression (39) relating the self-diffusion coefficient, the number density, and the parameters taking into account shear viscosity. Therefore, additional experimental studies of transport phenomena in liquid gallium, as well as determination and subsequent comparison of the values of the self-diffusion coefficient and shear viscosity, would be helpful for verifying the correctness of the Einstein–Stokes relation. It should be noted that intermediate expression (35) can be used to estimate the shear viscosity for the known behavior of quantity $\tilde{C}_T(k, 0)$ in the long-wavelength limit.

ACKNOWLEDGMENTS

The authors thank V.V. Brazhkin for helpful discussions.

Large-scale molecular-dynamics calculations were performed with the computer cluster of Kazan Federal University and the supercomputer of the Joint Supercomputer Center of the Russian Academy of Sciences.

This study was supported in part by the Russian Foundation for Basic Research (project nos. 14-02-00335-a and 15-02-06288-a).

REFERENCES

1. N. W. Ashcroft, Sci. Am. **221** (1), 72 (1969).
2. T. Iida and R. I. L. Guthrie, *The Physical Properties of Liquid Metals* (Clarendon, Oxford, 1993).
3. A. G. Lyapin, E. L. Gromnitskaya, O. F. Yagafarov, O. V. Stal'gorova, and V. V. Brazhkin, J. Exp. Theor. Phys. **107** (5), 818 (2008).
4. A. H. Narten, J. Chem. Phys. **56**, 1185 (1972).
5. Y. Waseda and K. Suzuki, Phys. Status Solidi B **49**, 339 (1972).
6. M. C. Bellissent-Funel, P. Chieux, D. Levesque, and J. J. Weis, Phys. Rev. A **39**, 6310 (1989).
7. O. F. Yagafarov, Y. Katayama, V. V. Brazhkin, A. G. Lyapin, and H. Saitoh, Phys. Rev. B: Condens. Matter **86**, 174103 (2012).
8. J. Frenkel, *Kinetic Theory of Liquids* (Dover, New York, 1955; Nauka, Leningrad, 1975).
9. S. F. Tsay and S. Wang, Phys. Rev. B: Condens. Matter **50**, 108 (1994).
10. G. Gong, G. L. Chiarotti, M. Parrinello, and E. Tosatti, Europhys. Lett. **21**, 469 (1993).
11. V. M. Nield, R. L. McGreevy, and M. G. Tucker, J. Phys.: Condens. Matter **10**, 3293 (1998).
12. J. Yang, J. S. Tse, and T. Iitaka, J. Chem. Phys. **135**, 044507 (2011).
13. K. H. Tsai, T.-M. Wu, and S. F. Tsay, J. Chem. Phys. **132**, 034502 (2010).
14. T. E. Faber, *An Introduction to the Theory of Liquid Metals* (Cambridge University Press, Cambridge, 1972).
15. A. V. Mokshin, Theor. Math. Phys. **183** (1), 449 (2015).
16. A. V. Mokshin, R. M. Yulmetyev R. M. Khusnutdinov, and P. Hänggi, J. Exp. Theor. Phys. **103** (3), 841 (2006).
17. R. M. Khusnutdinov, A. V. Mokshin, and R. M. Yul'met'ev, J. Exp. Theor. Phys. **108** (3), 417 (2009).
18. R. M. Khusnutdinoff, and A. V. Mokshin, JETP Lett. **100** (1), 39 (2014).
19. N. I. Eremin, *Gallium* (Metallurgiya, Moscow, 1964) [in Russian].
20. M. K. Lee, C. Tien, E. V. Charnaya, H. S. Sheu, and Y. A. Kumzerov, Phys. Lett. A **374**, 1570 (2010).
21. N. C. Chen and S. K. Lai, Phys. Rev. E: Stat. Phys., Plasmas, Fluids, Relat. Interdiscip. Top. **56**, 4381 (1997).
22. S. F. Tsay, Phys. Rev. B: Condens. Matter **48**, 5945 (1993).
23. R. M. Khusnutdinov and A. V. Mokshin, Bull. Russ. Acad. Sci.: Phys. **74** (5), 640 (2010).
24. V. N. Ryzhov, E. E. Tareeva, T. I. Shchelkacheva, and N. M. Shchelkachev, Theor. Math. Phys. **141** (1), 1443 (2004).
25. R. M. Khusnutdinoff, A. V. Mokshin, and I. I. Khadeev, J. Phys.: Conf. Ser. **394**, 012012 (2012).
26. R. M. Khusnutdinov, A. V. Mokshin, and I. I. Khadeev, J. Surf. Invest. **8** (1), 84 (2014).
27. I. Padureanu, A. Radulescu, A. Beldiman, M. Ion, A. G. Novikov, V. V. Savostin, and Zh. A. Kozlov, Physica B (Amsterdam) 276–278, 459 (2000).
28. N. M. Blagoveshchenskii, V. A. Morozov, A. G. Novikov, V. V. Savostin, and A. L. Shimkevich, Poverkhnost **6**, 10 (2006).
29. T. Scopigno, A. Filipponi, M. Krisch, G. Monaco, G. Ruocco, and F. Sette, Phys. Rev. Lett. **89**, 255506 (2002).
30. L. E. Bove, F. Formisano, F. Sacchetti, C. Petrillo, A. Ivanov, B. Dorner, and F. Barocchi, Phys. Rev. B: Condens. Matter **71**, 014207 (2005).
31. F. J. Bermejo, I. Bustinduy, S. J. Levett, J. W. Taylor, R. Fernández-Perea, and C. Cabrillo, Phys. Rev. B: Condens. Matter **72**, 104103 (2005).

32. S. Hosokawa, M. Inui, Y. Kajihara, K. Matsuda, T. Ichitsubo, W. C. Pilgrim, H. Sinn, L. E. González, D. J. González, S. Tsutsui, and A. Q. R. Baron, Phys. Rev. Lett. **102**, 105502 (2009).
33. V. Giordano and G. Monaco, Phys. Rev. B: Condens. Matter **84**, 052201 (2011).
34. N. M. Blagoveshchenskii, A. G. Novikov, A. V. Puchkov, and V. V. Savostin, JETP Lett. **100** (5), 340 (2014).
35. N. M. Blagoveshchenskii, A. G. Novikov, A. V. Puchkov, and V. V. Savostin, Crystallogr. Rep. (2015) (in press).
36. S. Hosokawa, M. Inui, Y. Kajihara, S. Tsutsui, and A. Q. R. Baron, J. Phys.: Condens. Matter **27**, 194104 (2015).
37. D. K. Belashchenko, Russ. J. Phys. Chem. A **86**, 779 (2012).
38. D. K. Belashchenko, Phys.—Usp. **56** (12), 1176 (2013).
39. A. V. Mokshin, A. V. Chvanova, and R. M. Khusnutdinov, Theor. Math. Phys. **171** (1), 541 (2012).
40. A. V. Mokshin, R. M. Yulmetyev, R. M. Khusnutdinov, and P. Hänggi, Phys. Solid State **48** (9), 1760 (2006).
41. A. V. Mokshin, S. O. Zabegaev, and R. M. Khusnutdinoff, Phys. Solid State **53** (3), 570 (2011).
42. N. Blagoveshchenskii, A. Novikov, A. Puchkov, V. Savostin, and O. Sobolev, EPJ Web Conf. **83**, 02018 (2015).
43. A. Novikov, Yu. Lisichkin, and N. Fomichev, Zh. Fiz. Khim. **60**, 1337 (1986).
44. S. Hosokawa, W.-C. Pilgrim, H. Sinn, and E. Alp, J. Phys.: Condens. Matter. **20**, 114107 (2008).
45. N. H. March, *Liquid Metals: Concepts and Theory* (Cambridge Univ. Press, Cambridge, 1990).
46. J. A. Prins and H. Petersen, Physica (Amsterdam) **3**, 147 (1936).
47. J.-P. Hansen and L. Verlet, Phys. Rev. **184**, 151 (1969).
48. H. R. Wendt and F. F. Abhraham, Phys. Rev. Lett. **41**, 1214 (1978).
49. Y. Waseda, *The Structure of Non-Crystalline Materials: Liquids and Amorphous Solids* (McGraw-Hill, New York, 1980).
50. P. R. ten Wolde, M. J. Ruiz-Montero, and D. Frenkel, J. Chem. Phys. **104**, 9932 (1996).
51. P. J. Steinhardt, D. R. Nelson, and M. Ronchetti, Phys. Rev. B: Condens. Matter **28**, 784 (1983).
52. A. V. Mokshin and J.-L. Barrat, Phys. Rev. E: Stat., Nonlinear, Soft Matter Phys. **77**, 021505 (2008).
53. J. P. Hansen and I. R. McDonald, *Theory of Simple Liquids* (Academic, New York, 2006).
54. R. M. Khusnutdinoff and A. V. Mokshin, J. Non-Cryst. Sol. **357**, 1677 (2011).
55. R. M. Khusnutdinoff and A. V. Mokshin, Physica A (Amsterdam) **391**, 2842 (2012).
56. R. M. Khusnutdinoff, A. V. Mokshin, and I. D. Takhaviev, Phys. Solid State **57** (2), 412 (2015).
57. K. Trachenko and V. V. Brazhkin, submitted to Rev. Mod. Phys. (2015).
58. A. V. Mokshin, R. M. Yulmetyev, R. M. Khusnutdinoff, and P. Hänggi, J. Phys.: Condens. Matter **19**, 046209 (2007).
59. W. Schirmacher, T. Scopigno, and G. Ruocco, J. Non-Cryst. Sol. **407**, 133 (2015).
60. P. Jedlovszky, G. Garberoglio, and R. Vallauri, J. Phys.: Condens. Matter **22**, 284105 (2011).
61. N. Ohtori and Y. Ishii, Phys. Rev. E: Stat., Nonlinear, Soft Matter Phys. **91**, 012111 (2015).
62. R. Zwanzig, J. Chem. Phys. **79**, 4507 (1983).
63. *Physics of Simple Liquids*, Ed by H. Temperley, J. Rowlinson, and G. Rushbrook (North-Holland, Amsterdam, The Netherlands, 1968; Mir, Moscow, 1971).
64. A. V. Mokshin and R. M. Yulmetyev, *Microscopic Dynamics of Simple Liquids* (Center of Innovation Technologies, Kazan, 2006) [in Russian].
65. A. V. Mokshin and J.-L. Barrat, Phys. Rev. E: Stat., Nonlinear, Soft Matter Phys. **82**, 021505 (2010).

Translated by N. Wadhwa